REPORT DOCUMENTATION PAGE

Form Approved
OMB No. 0704-0188

1. AGENCY USE ONLY *(Leave Blank)*	2. REPORT DATE	3. REPORT TYPE AND DATES COVERED
	December 21, 2004	Final: 12/30/00 - 09/30/04

4. TITLE AND SUBTITLE
Multispectral Remote Sensing and COAMPS Model Analysis Methods for Marine Cloud Structure, Entrainment Processes and Refractivity Effects

5. FUNDING NUMBERS
N00014-01-1-0295

6. AUTHORS
Melanie A. Wetzel
Steven K. Chai
Darko R. Koracin

7. PERFORMING ORGANIZATION NAME(S) AND ADDRESS(ES)
Desert Research Institute
University & Community College System of Nevada
2215 Raggio Parkway
Reno, NV 89512-1095

8. PERFORMING ORGANIZATION REPORT NUMBER
N/A

9. SPONSORING / MONITORING AGENCY NAME(S) AND ADDRESS(ES)
Office of Naval Research
800 North Quincy Street
Arlington, VA 22217-5660

10. SPONSORING / MONITORING AGENCY REPORT NUMBER

11. SUPPLEMENTARY NOTES
None

12a. DISTRIBUTION / AVAILABILITY STATEMENT
Unlimited

12b. DISTRIBUTION CODE

13. ABSTRACT *(Maximum 200 words)*

The primary goal of this research is advancement in the utilization of satellite remote sensing methods with mesoscale simulation models for improved prediction of marine stratus and boundary layer structure. Related goals include the study of marine stratus evolution and analysis of microwave refractivity at the interface of the cloudy marine layer and the free troposphere. High accuracy for short-term prediction of cloud and inversion structure in marine environments is required for Navy operations, particularly in the vicinity of stratus and fog decks. Knowledge related to the probable evolution of cloud fractional cover, cloud liquid water profiles, the presence of precipitation and microwave ducting conditions are essential for effective logistical decision-making. Our research objectives focus on the optimum utilization of parameter fields from the Navy's COAMPS and other mesoscale forecasting models with geostationary satellite data for monitoring and predicting the short-term physical characteristics of the marine boundary layer cloud and thermodynamic conditions.

14. SUBJECT TERMS
Remote sensing,COAMPS, numerical modeling, simulations, coastal marine layer, diurnal effects, stratus, entrainment, refractivity, satellite, inversion

15. NUMBER OF PAGES
18

16. PRICE CODE

17. SECURITY CLASSIFICATION OF REPORT	18. SECURITY CLASSIFICATION OF THIS PAGE	19. SECURITY CLASSIFICATION OF ABSTRACT	20. LIMITATION OF ABSTRACT
Unclassified	Unclassified	N/A	

FINAL REPORT
to
Office of Naval Research

for the project entitled

"Multispectral Remote Sensing and COAMPS Model Analysis Methods for Marine Cloud Structure, Entrainment Processes and Refractivity Effects"

Submitted 21 December 2004

Melanie A. Wetzel
Division of Atmospheric Sciences, Desert Research Institute
2215 Raggio Parkway, Reno NV 89512-1095
phone: (775) 674-7024 fax: (775) 674-7016 email: wetzel@dri.edu

Steven K. Chai
Division of Atmospheric Sciences, Desert Research Institute
2215 Raggio Parkway, Reno NV 89512-1095
phone: (775) 674-7070 fax: (775) 674-7007 email: chai@dri.edu

Darko R. Koracin
Division of Atmospheric Sciences, Desert Research Institute
2215 Raggio Parkway, Reno NV 89512-1095
phone: (775) 674-7091 fax: (775) 674-7016 email: darko@dri.edu

Award Number: N00014-01-1-0295

1. Introduction

The primary goal of this research is advancement in the utilization of satellite remote sensing methods and mesoscale simulation models for improved prediction of marine stratus and boundary layer structure. Related goals include the study of marine stratus evolution and analysis of microwave refractivity at the interface of the cloudy marine boundary layer and free troposphere. High accuracy for short-term prediction of cloud and inversion structure in marine environments is required for Navy operations, particularly in the vicinity of stratus and fog decks. Knowledge on the probable evolution of cloud cover, cloud vertical profile and microwave refractivity at the top of the marine boundary layer (MBL) is essential for effective logistical and tactical decision-making. Our research objectives focus on the optimum utilization of parameter fields from the Navy's COAMPS (Coupled Ocean/Atmosphere Mesoscale Prediction System) and other mesoscale forecasting models with geostationary satellite data for monitoring and predicting the short-term physical characteristics of boundary layer cloud and thermodynamic conditions in the vicinity of cloud top.

The objectivew of this project include integrated analysis of satellite, aircraft and model case study datasets from field measurement programs in both day and night conditions. A successful collaboration was established between scientists at DRI, NRL, University of Wyoming, UCLA and other groups. Datasets have been obtained during the DYCOMS-II (Dynamics and Chemistry of Marine Stratocumulus-II) project (Stevens et al., 2003) and the COSAT (COAMPS Operational Satellite and Aircraft Test) field program (Wetzel *et al.*, 2001). These data have been used to evaluate marine boundary layer structure as observed with satellite retrieval techniques and model forecasts. The data are also used to identify model-derived fields which can contribute information content and reliability of satellite-obtained information.

Several excellent datasets on the structure of night-time offshore stratus were collected during the DYCOMS-II and COSAT experiments. COAMPS model gridded output results were obtained from NRL from real-time simulations conducted during DYCOMS-II, and MM5 modeling has been conducted at DRI for the same cases. Research studies include analysis of microphysical and thermodynamic structure using satellite and aircraft data obtained during research flight missions.

2. Project Results

2.1 Satellite Data for Initialization and Diagnosis of Boundary Layer Parameters

Application of GOES multispectral satellite data collected during the DYCOMS-II nighttime research flights has allowed development and evaluation for retrieval techniques and improvement in model initial conditions. At night, only thermal infrared and near-infrared satellite observations are available, which reduces the information available for retrieval of cloud microphysical parameters. We have utilized a combination of aircraft and satellite data to investigate cloud structure for multiple research flights during July 2001.

Figure 1 shows the results of an estimation procedure that combines GOES 11 micron and 3.9 micron channel brightness temperatures, sea surface temperature (obtained from TRMM satellite data and field measurements), satellite-observed cloud top temperature, and typical lapse rates in the MBL, to map cloud droplet mean diameter in the marine stratus layer using curve fitting to radiative transfer forward model results for varied cloud droplet distributions (Wetzel et al., 2001). The spatial variation and magnitudes of estimated droplet size during a flight circle (indicated in red on the figure) compares very closely to aircraft measurements in the upper portion of the cloud layer. The major factor in this spatial variation is the difference in the spectral radiance emitted upward from the cloud layer associated with changes in typical droplet size. The 11 micron – 3.0 micron brightness temperature difference (BTD) increases as droplet size decreases due to emissivity differences between these two wavelengths.

It is of interest to know whether these signatures also indicate whether cloud droplet growth has reached drizzle stage. The aircraft carried the University of Wyoming cloud radar on these research flights. Figure 2 depicts the vertical profile of radar reflectivity along the flight circle shown in Figure 1. Reflectivities greater than -15 dBZ (orange and shading in Figure 2)

have vertical streaks indicating probably drizzle shafts. Comparisons of vertically-averaged radar reflectivity for the cloud layer along the flight path have been made to satellite-observed BTD values, as shown in Figure 3. This scatterplot indicates an increase in radar reflectivity above -15 dBZ is associated with BTD smaller than 2.5 K, which is equivalent to a droplet diameter of approximately 17 μm.

The radar vertical profiles have been evaluated with aircraft microphysical measurements, and in collaboration with Dr. Gabor Vali (University of Wyoming) to document the occurrence of drizzle. Figure 4 is a composite time series of the aircraft microphysics, radar, aircraft-detected cloud top temperature and satellite-observed cloud top temperature data for this flight segment. It is not possible to directly compare the time series of in-cloud microphysics to the parameters observed while the aircraft was flying above cloud for radar scanning, but flight circles very close in time, flown just below cloud top, indicate the range of droplet sizes shown in the Figure 1 estimates. In a related study, the PI collaborated with Dr. Cynthia Twohy and others in case study analysis from DYCOMS-II data (Twohy et al., 2005, in press) where reductions in droplet size were linked to reduction in drizzle water concentration.

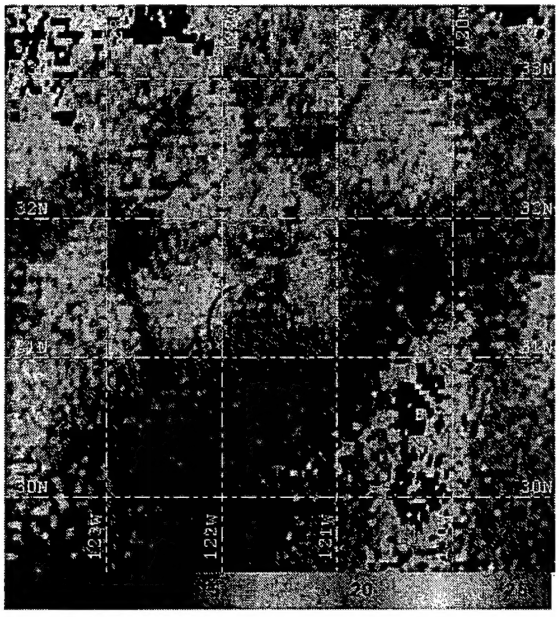

Figure 1. Mapped distribution of cloud droplet mean diameter (μm) estimated from GOES brightness temperature difference data for the 1145 UTC satellite image time on 10 July 2001 over the DYCOMS II study region. The red overlay designates the aircraft track (traveling counter-clockwise) during 1145-1214 UTC. Droplet diameter values range from near 18 μm (light green) near the beginning and end of the flight segment to as low as 13 μm (dark blue) in the middle period of this segment.

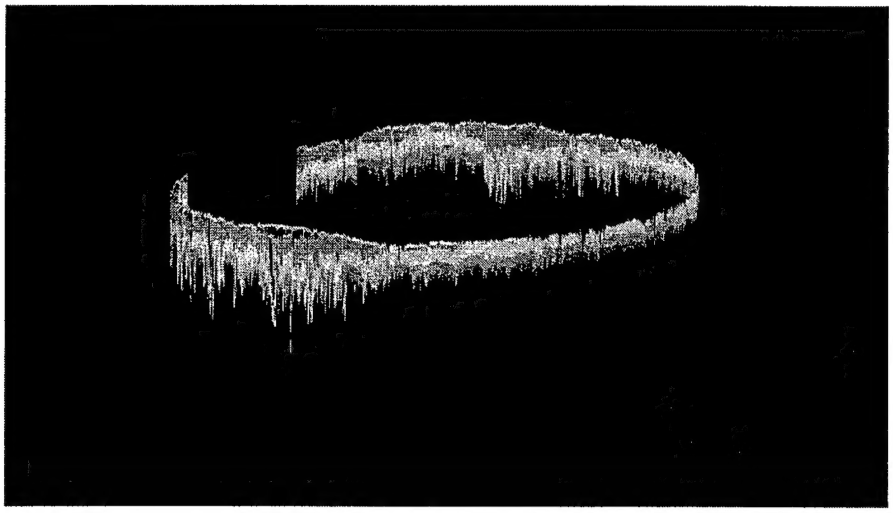

Figure 2. Vertical profile of the King Air radar reflectivity for the 10 July 2001 flight segment that is shown in Figure 1. The periods of enhanced radar reflectivity and vertically extensive radar echo generally correspond to larger concentrations and sizes of cloud droplets and greater likelihood of drizzle. Radar data courtesy of Dr. Gabor Vali, University of Wyoming.

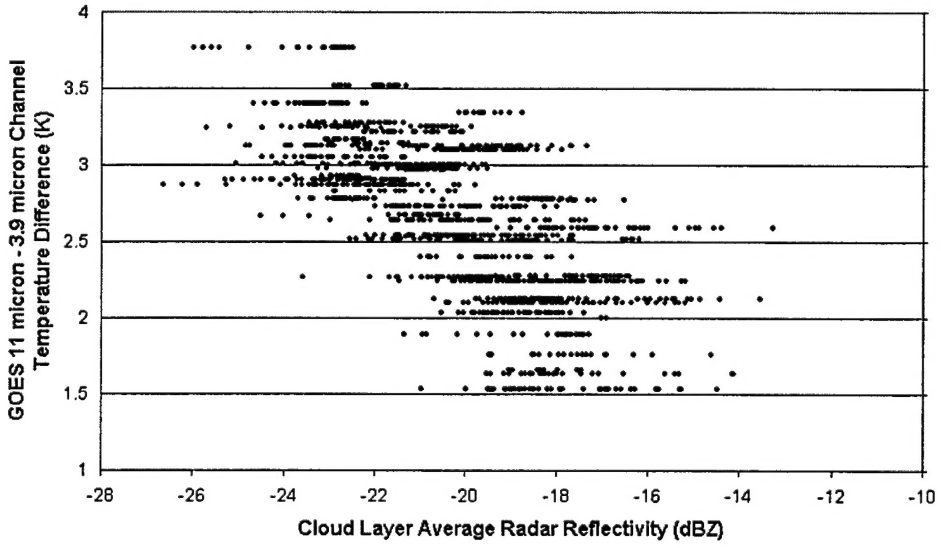

Figure 3. Scatterplot of cloud layer average radar reflectivity and satellite-observed brightness temperature differences for the 10 July 2001 flight segment shown in Figure 1. The periods of enhanced radar reflectivity correspond to smaller brightness temperature differences in the satellite signature and larger estimates of droplet size. Radar data courtesy of Dr. Gabor Vali, University of Wyoming.

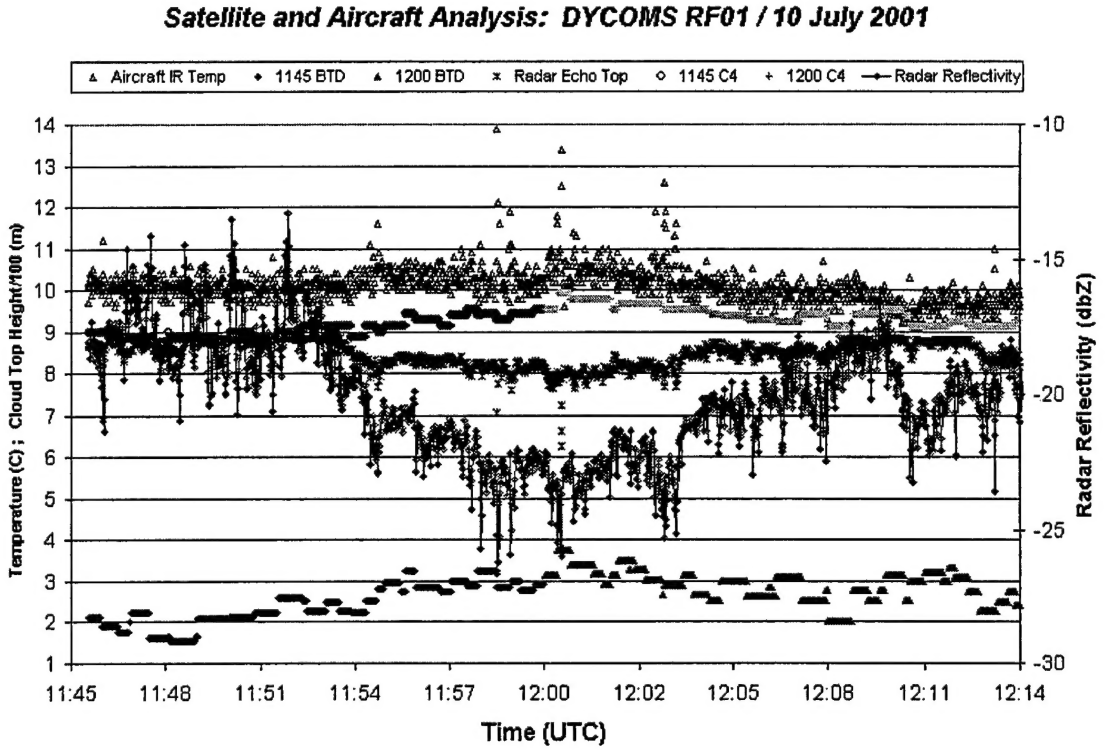

Figure 4. Time series of in situ and remotely sensed cloud parameters for the 10 July 2001 flight segment shown in Figure 1. The BTD and Channel 4 data are from GOES; the Aircraft IR Temperature was obtained with an infrared sensor viewing downward from the aircraft toward cloud top. Radar and other aircraft data courtesy of Dr. Gabor Vali, University of Wyoming.

2.1.1 Satellite-derived Boundary Layer Height and Refractivity

We have conducted intercomparison and validation of the COAMPS and MM5 mesoscale prediction models, satellite remote sensing analyses, and development of new methods to merge satellite observations with model simulations. A technique for assimilating satellite-derived sea surface temperature (from TRMM satellite data) and cloud top temperature (from GOES satellite data) has been applied to model simulations and estimates of MBL thermodynamic structure and microwave refractivity. Information on the vertical and horizontal distribution of modified refractivity can provide excellent diagnosis of the microwave signal trapping that often occurs due to temperature and humidity gradients at the top of the MABL (Haack and Burk, 2001). However, temperature and humidity profile observations in the MABL are sparse over the majority of oceanic regions, and hence the motivation to incorporate satellite remote sensing data where possible, and the use of these data as input to model simulations. Modified Refractivity (M) is defined as:

$$M = \frac{77.6}{T}\left(P + 4810\frac{e}{T}\right) + \left(\frac{Z}{R_e} \times 10^6\right)$$

where T= air temperature (K), P= pressure (mb), e= water vapor pressure (mb), Z = altitude (m), and R_e= mean radius of earth (m).

MM5 simulations have been conducted which define the initial MABL temperature profile using GOES cloud top temperature, TRMM sea surface temperature, and applying an adiabatic lapse rate to determine the height of the inversion base. This method improves the short-term prediction of temperature and humidity in the MABL (see Figure 5 and Figure 6), so that the MM5 simulations follow the observed profiles more closely than COAMPS simulations run in real-time during the DYCOMS-II field project. Note that the MM5 simulations also benefited from greater vertical resolution in the MABL. However, the COAMPS forecasts were run in continuous mode and demonstrate a much better representation of the humidity profile (Figure 6) above the inversion, as compared with the MM5 simulations that were run in "cold-start" mode each day. This has a strong influence on the predicted refractivity profile (Figure 7). While the M profile predicted by MM5 is improved up to the inversion base, the MM5 did not capture the negative M gradient at the inversion. We are continuing the development of model simulations with the satellite-enhanced MABL profile data in multiple cycles as in operational mode, to better characterize the dry layer above the subsidence inversion.

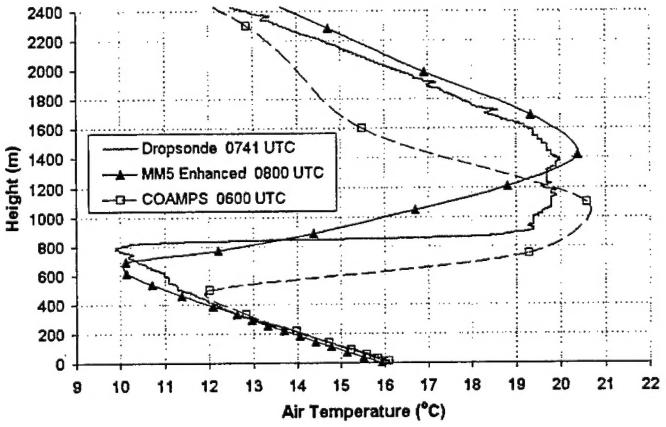

Figure 5. Vertical profiles of air temperature obtained from model simulations and aircraft dropsonde measurements during the DYCOMS-II case study on 10 July 2001. The MM5 predicted profile was enhanced by use of initial conditions obtained from GOES satellite cloud top temperature and TRMM satellite sea surface temperature.

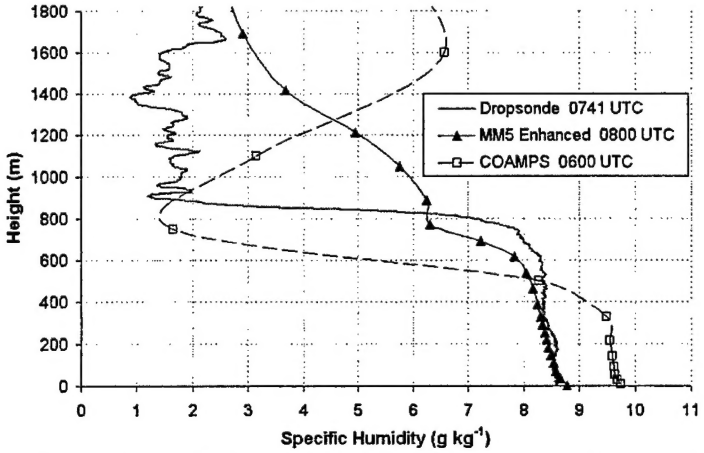

Figure 6. Vertical profiles of specific humidity obtained from model simulations and aircraft dropsonde measurements during the DYCOMS-II case study on 10 July 2001.

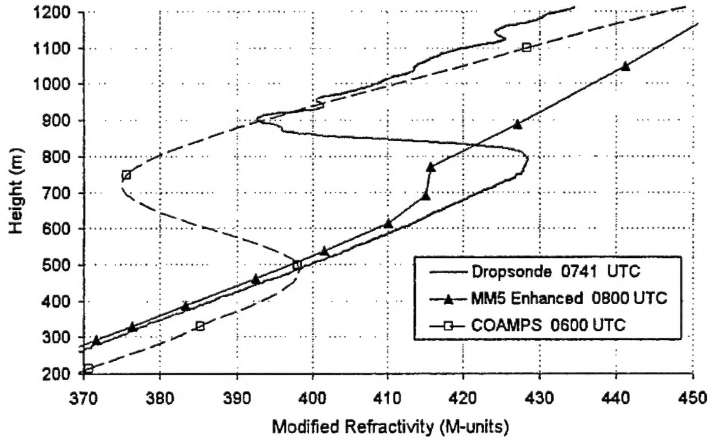

Figure 7. Vertical profiles of Modified Refractivity obtained from model simulations and aircraft dropsonde measurements during the DYCOMS-II case study on 10 July 2001, calculated from model conditions of humidity and temperature. The profile of refractivity is improved within the MABL but does not adequately represent the negative gradient in the 800-900 m layer associated with the dry air above the inversion.

Additional refinement in these model simulations was obtained by inserting one additional grid nest in the model domain with a horizontal resolution of 1 km. This addition improved significantly the simulated thermal structure (Figure 8). Uncertainty and errors in the thermal structure induce errors in the prediction of cloudiness. Figure 9 demonstrates how the choice of the initialization data fields influences the predicted vertical profiles within and above the MBL, and that the increased horizontal grid resolution produces a more accurate representation of the cloud layer. The improvement is most notably present in depicting the inversion base and cloud top height. Accurate cloud top height and temperature is critical for

proper treatment of radiation fluxes and prediction of the diurnal evolution of the MBL. Further model development at high grid resolution will contribute to better forecasts of microwave refractivity profiles as well as the radiative flux profiles and MBL diurnal cycle that influences the refractivity environment.

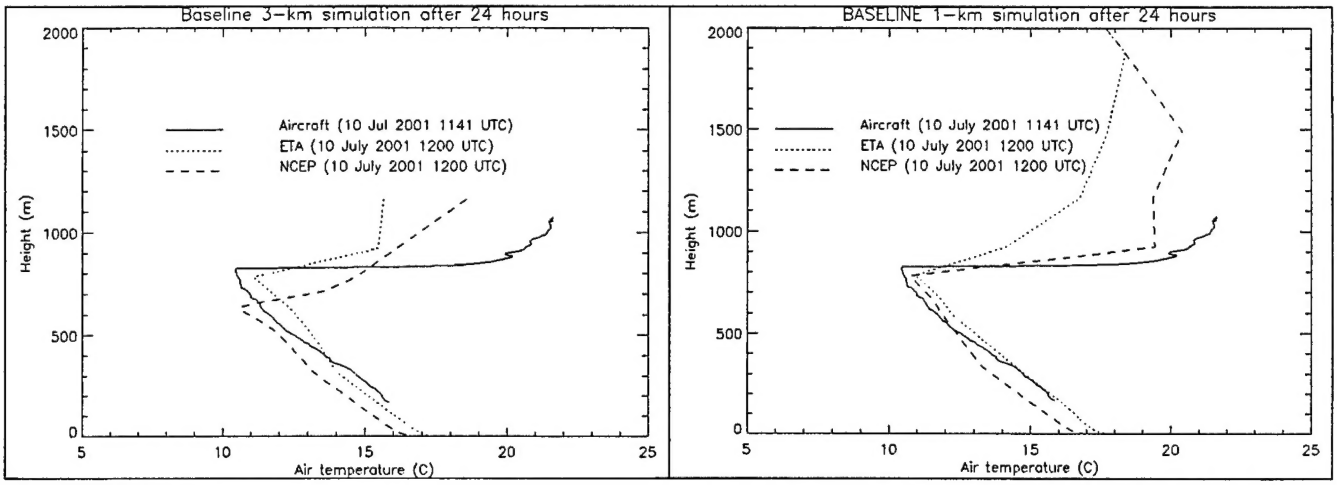

Fig. 8. Vertical profiles of ambient temperature (°C) as measured by aircraft and simulated by MM5 with horizontal resolutions of 3 km (left panel) and 1 km (right panel) on 10 July 2001.

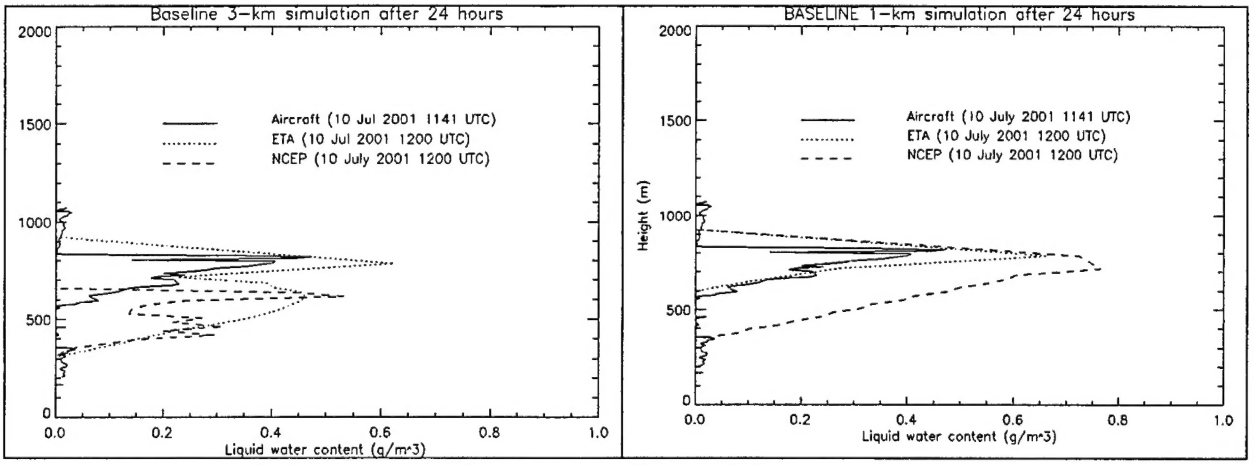

Fig. 9. Vertical profiles of the liquid water content as measured by aircraft and simulated by MM5 with horizontal resolutions of 3 km (left panel) and 1 km (right panel) on 10 July 2001.

2.2 Utilization of Cloud Climatology Data for COAMPS Verification Studies

The PI has collaborated with Tracy Haack of the Naval Research Laboratory (Monterey) in use of satellite cloud climatology data for intercomparison of seasonal variations in marine cloud layer structure with COAMPS model results. The seasonal variability of marine cloud

layer characteristics was examined by use of the International Satellite Cloud Climatology Project (ISCCP) datasets available from NASA (http://isccp.giss.nasa.gov/). The ISCCP cloud detection and gridding procedure has been validated (Rossow and Garder, 1993), and has been utilized in previous studies of marine stratiform cloud climatology (Rozendaal et al., 1995). The ISCCP DX 30-km resolution dataset available for North America provided gridded daily cloud distributions at 3-hourly intervals (0, 3, 6, ... 18 UTC), as derived from the ISCCP processing methods using GOES-West multi-channel digital image data.

All days in January, April, July and October 1999 were composited to obtain monthly average cloud top temperature (CTT) for cloudy time periods in each of those four months. Only cloudy grid cells were included in the composite, and these were restricted to CTT $\geq$ 271 K to limit analysis to situations with low cloud and no overlying cloud, so that the actual CTT of the marine layer cloud was observable. The model data analysis applied the same cloud top temperature threshold to accurately simulate the information available from the satellite observations. Cloud top temperature for marine stratiform cloud layer varies as the MBL inversion depth and vertical temperature structure changes, in response to air mass transitions as well as dynamic features of the coastal region that are modulated by circulation patterns and land-sea contrasts. The satellite data analysis offers a means of confirming the ability of the model to represent these regional and mesoscale processes through their impacts on seasonal and geographic cloud patterns.

A research article near completion (Haack et al., 2004) describes the results of the COAMPS and GOES analyses. The satellite-derived spatial distributions of MBL cloud top temperature for the four months (Figure 10) indicate significant seasonal variation in the geographic patterns and magnitudes of CTT. The temperature range in January over the analysis domain is 273-280 K, with a band of warmest CTT extending westward across the region from the southern California coastline. The April spatial pattern is very similar to that obtained from model results for January, with coolest temperatures hugging the northern coastline and an east-west band of warmest temperatures in the southern section of the analysis region. The CTT field for April is similar to that for January, with an overall cooling in CTT in the southern extent of the analysis region. The July and October CTT fields are notably warmer, with CTT values reaching > 281 K over much of the southern portion of the region. A distinct difference between cloud layer features between summer and fall is the cooler CTT for October along the coast in the northern third of the analysis region, while the coolest cloud tops are found offshore during summer.

The overall magnitudes for model results are approximately 2 K warmer than CTT values in corresponding areas of the satellite results. This offset is observed for each of the four months. This difference could be attributed to inadequate representation of water vapor absorption/emission by precipitable water above cloud top in the ISCCP analysis of CTT. Figure 11 demonstrates the influence of water vapor column amount on the effective CTT detected by the GOES thermal infrared sensor. In this example, the ambient cloud top temperature is 287 K, and while conditions of optically thin cloud cause a warm bias for satellite observations, the effect of atmospheric extinction above cloud is more important for optically thick cloud. This creates a cool bias in effective cloud top temperature that increases with the magnitude of column

water vapor, and can create a difference of almost 2 K if not properly attributed in the ISCCP data grids for CTT. A second source of discrepancy in the CTT comparisons is the vertical resolution of the model, which may not represent the full vertical extent of the marine layer cloud.

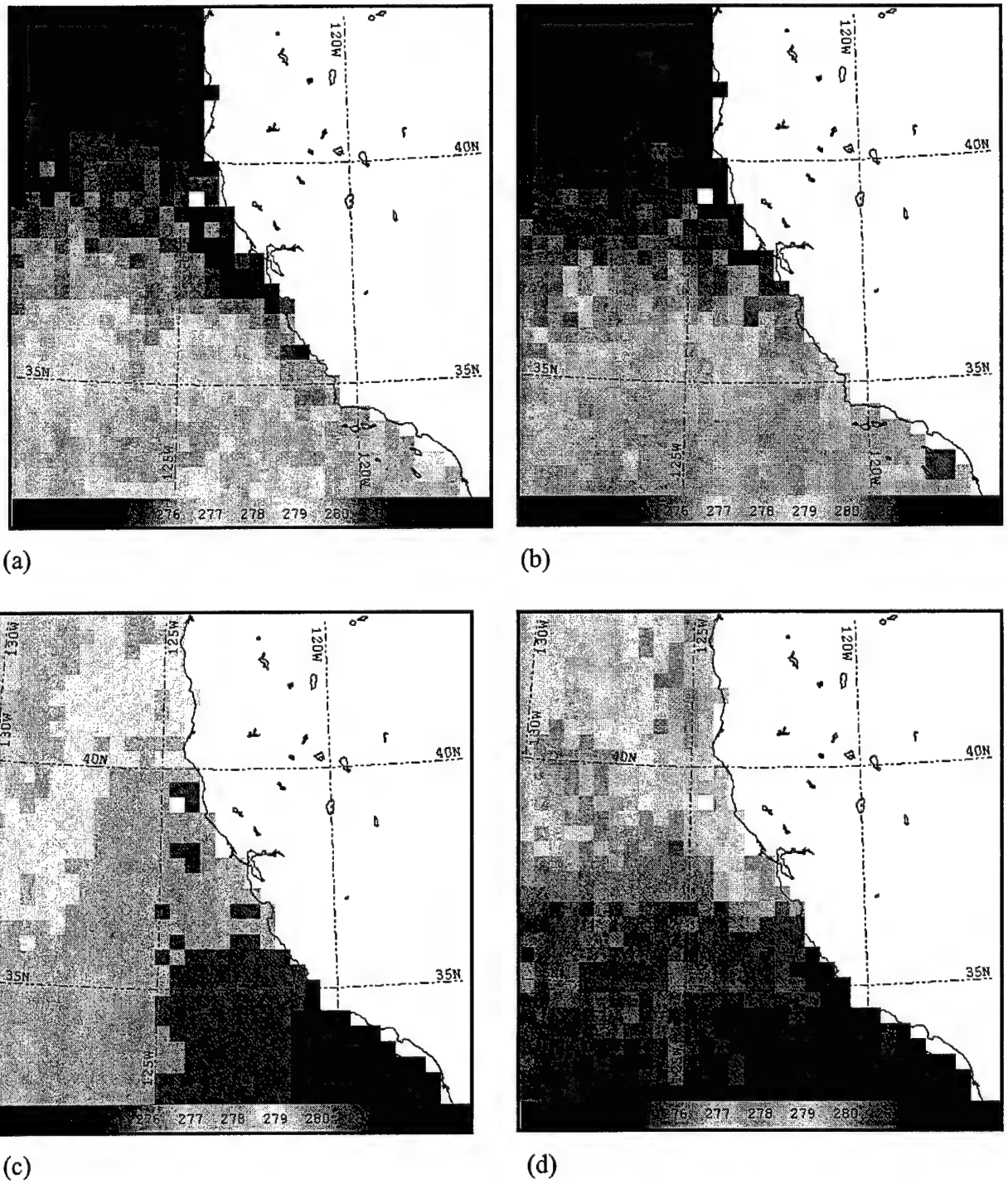

Figure 10. Monthly average cloud top temperature for marine layer cloud derived from ISCCP archive datasets, for (a) January, (b) April, (c) July and (d) October 1999.

Locally warm CTT values near the Channel Islands offshore southern California seen in each of the four months are indicative of fog and thin stratus in this area. The satellite data are additionally vulnerable to the effects of broken low cloud, when grid cells are identified as cloudy, but there is correspondence between the model and satellite cloud fields for this coastal area. The satellite data are also limited in their analysis of cloud cover immediately adjacent to the coastal zone, due to cloud classification difficulties where land and ocean coexist within a single satellite grid cell. Aside from these minor restrictions, the satellite-derived marine cloud fields correspond well with the model results with respect to seasonal variability and geographic patterns in CTT.

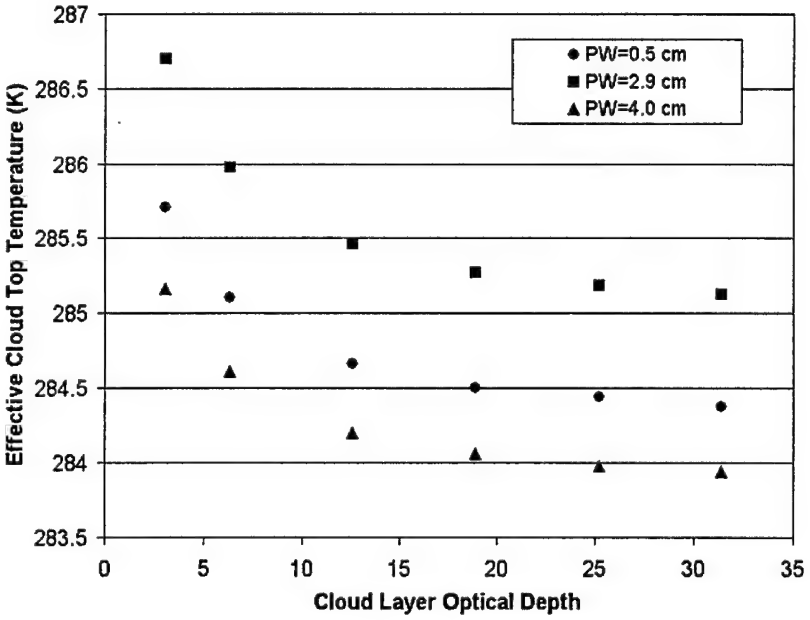

Figure 11. Calculated effective cloud top temperature (K) for varied conditions of column precipitable water (PW) that would be observed using the GOES-West thermal infrared imaging channel.

2.3 Analysis of Entrainment Processes for COSAT and DYCOMS-II Experiments

Entrainment processes are critical to the evolution of marine boundary layer clouds (Lilly, 1968, Randall, 1980, Deardorff, 1976, 1980, Telford and Chai, 1984, Bretherton et al., 1999, Lock and MacVean, 1999). The complexity caused by the presence of cloud introduces a set of feedbacks among the rate of entrainment, radiative and evaporative cooling, surface fluxes, turbulence, and precipitation. The short length scale of the entrainment processes (Bretherton et al., 1999 and Stevens et al., 2000) cannot be accurately represented by an operational meteorological model. A method of treating boundary layer entrainment developed by Telford and Chai (1984) has been applied in a one-dimensional model with the same cloud microphysics parameterization as the COAMPS for study of the cloud top entrainment processes. The method

is based on the use of the entrainment instability profile (which is the wet-bulb potential temperature profile) in the atmospheric layer immediately above the top of the boundary-layer cloud. The entrained air must have a lower wet-bulb potential temperature than that of the cloudy air in order to have the entrained air cooled to a lower temperature and sink into the cloud layer. This is the so called the entrainment instability condition. Otherwise, the entrained air will be float at the top of the cloudy layer and form a buffer layer that prevents further entrainment. The entrainment rate will be proportional to the local turbulent potential energy and the amount of air entrained will depend on the entrainment instability profile of the air above the cloud top.

The COSAT (Wetzel et al., 2001) and DYCOMS-II (Stevens et al., 2003) field programs provided a very useful dataset for marine stratus and stratocumulus offshore Oregon and southern California. The objective of the DYCOMS-II program was to better understand the physics and dynamics of nocturnal marine stratocumulus. Toward this end special flight strategies were employed to optimize estimates of entrainment velocities at cloud top and cloud microphysics. Detailed data analyses leading to our conclusion are following.

Uniform cloud fields topping a well-mixed layer characterized almost every flight mission during DYCOMS-II. Analyses of the airborne data have included use of a specialized thermodynamic diagram for absolute potential temperature (θ_A), which is the temperature of an air parcel adiabatically lowered to 100 kPa with inclusion of the liquid water content in that parcel. The analyses indicate that the net radiative loss at cloud top effectively cools the cloud layer, resulting in a layer with cooler θ_A than that of the air below cloud base. Hydrostatic instability between the cloud layer and the air below is thus created. With some triggering mechanism, intermittent convection will take place in the marine boundary layer and a uniform absolute potential temperature throughout the boundary layer would then be reestablished. This radiative cooling effect impacts not only the cloud dynamics but also the cloud microphysical evolution.

The cloud-top radiative cooling effect was identified in the DYCOMS-II research flights. Comparison of two vertical soundings observed during the first research flight demonstrates the thermodynamic analysis procedure. Figure 12(a) shows the liquid water mixing ratio (r_v) profile observed by NCAR C130 during the first research flight (RF01), third profile sounding (PF03). This is a profile ascending through the cloud layer. Cloud base and top heights can be easily identified in this figure. Active cloud-top entrainment can be interpreted from the occasional spikes of smaller r_v values and from the slope of the profile. Figure 12(b) shows the profile of the absolute potential temperature (θ_A, solid line) and the wet-bulb potential temperature (θ_W, dashed).

The marine boundary layer appears well mixed since both profiles are almost vertical lines. Newly entrained parcels have a slightly higher θ_A and cooler θ_W. This can be seen more clearly on the θ_W vs. θ_A diagram (Telford and Chai, 1993). In this type of thermodynamic diagram, the θ_W vs. θ_A diagram, the dotted sloping lines are constant total mixing ratio lines and the solid sloping lines are the constant saturation pressure lines. These quantities, as well as θ_A and θ_W, are conserved during adiabatic motion of an air parcel with or without liquid water.

Figure 13 shows the RF01/PF03 data on the θ_W vs. θ_A diagram. All the points in the marine boundary layer are clustered in a small region ($\theta_W \approx 13.5^oC$, $\theta_A \approx 16^oC$) on this diagram, indicating that the layer is well mixed. Newly entrained parcels would be easily identified as they have lower r_v and θ_W values but higher θ_A values.

Figure 14(a) shows the liquid water mixing ratio profile during RF02/PF04 (a descending sounding through the cloud layer), taken about 40 minutes after the previous sounding (PF03). Both the cloud base and top heights are similar to the previous sounding. Entrainment is still active during this time period. However, the θ_A and θ_W profiles (Figure 14(b)) show a cooling in the cloud layer and in the region immediately below cloud base. The θ_W vs. θ_A diagram of this profile shows that the data points in the cooled layer are aligned parallel to a constant total mixing ratio line. This is an indication that the cooling is caused by long-wave radiative cooling from cloud top. In this figure, data points near cloud top have a saturation pressure level near 1000 mb, which explains the nearly equal values of θ_A and θ_W shown in Figure 15.

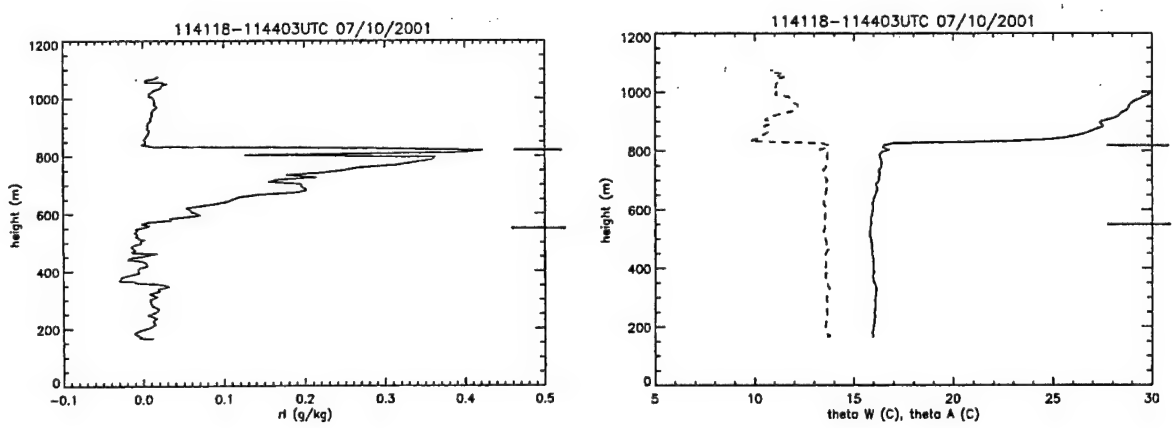

Figure 12. (a) Liquid-water mixing ratio observed during DYCOMS-II Research Flight 01, profile No. 3 (RF01/PF03). Cloud base and top heights are identified by short horizontal lines on the right vertical axis. (b) The profiles of absolute potential temperature (solid curve) and wet-bulb potential temperature (dashed curve) of RF01/PF03.

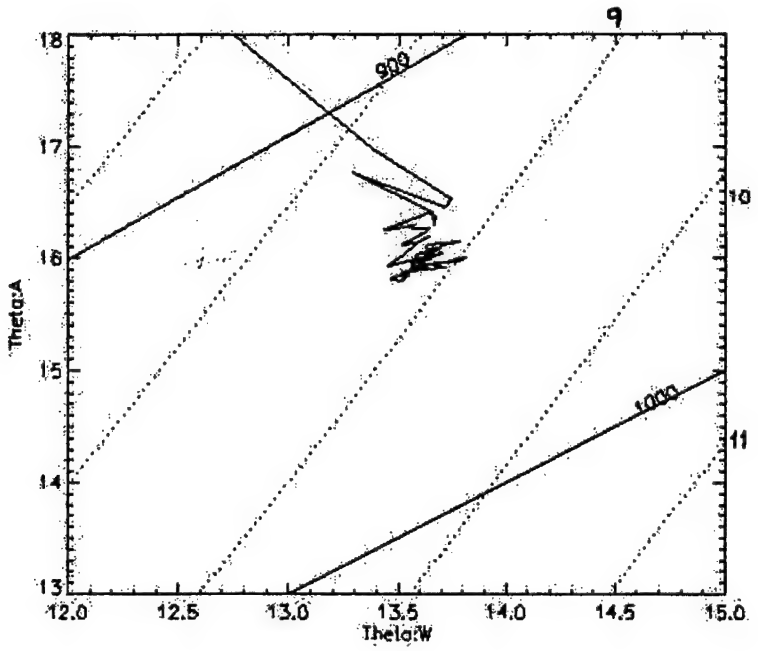

Figure 13. This θ_W-θ_A thermodynamic diagram displays the RF01/PF03 data. Since the boundary layer is well mixed, the data points measured below the capped temperature inversion are clustered in a small region on this diagram. Solid sloping lines represent constant saturation pressure and the dotted sloping lines represent constant total mixing ratio.

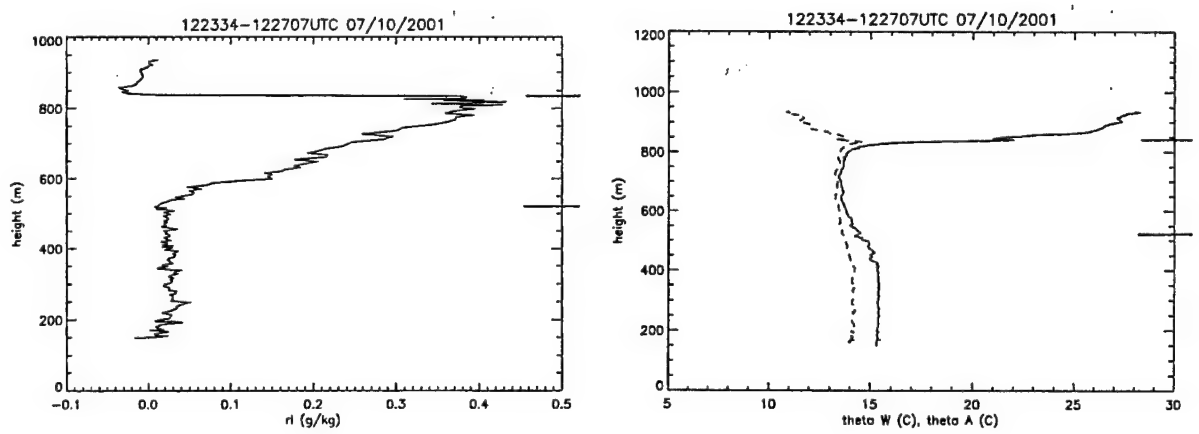

Figure 14(a) and (b). Same as Figure 12 but for RF01/PF04.

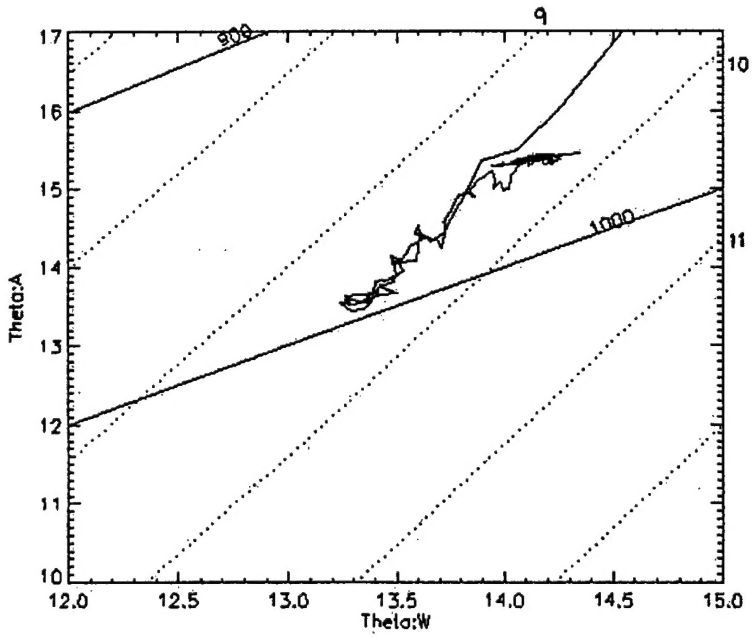

Figure 15. Same as Figure 13 but for RF01/PF04. The data points in the cooled absolute potential temperature region are aligned along a constant total mixing ratio line (dotted lines) indicate that radiative cooling is the main cause of the cooling.

From analyzing the DYCOMS-II airborne data, the above-mentioned radiative cooling signatures – a layer of air, immediately under the inversion base, with cooler θ_A and θ_W values than the air below while the total mixing ratio remains as a constant throughout the boundary layer – were found periodically in all the research fights. This may be an indication of an intermittent nature of convection in the marine boundary layer. The effect of radiative cooling gradually diffuses downward by turbulent mixing, leading to a hydrostatically unstable layer. Any triggering mechanism may initiate the convective motion that leads to a well-mixed marine boundary layer. The data suggests a link between these cooling signatures and the rates of cloud-top radiative cooling. The cooling rate at cloud top for PF03 is $-7K\ hr^{-1}$ while for PF04 it is $-20\ K\ hr^{-1}$. The cooling signature generally appears when the cloud-top heating rate less than $-15\ K\ hr^{-1}$.

The intermittent nature of convection in the marine boundary layer and the radiative cooling effect are important in both cloud dynamics and microphysics. During periods with no convection through the whole boundary layer, the effect of entrainment on cloud droplet spectra broadening (Telford and Chai, 1980, Telford and Wagner, 1981, and Telford et al, 1984) may become effective and lead to faster drizzle formation. The effect of the entity-type entrainment mixing will be lost whenever the surface driven convection (either by water vapor flux or heat flux) mixes through the whole marine boundary layer. However, when the surface driven convection is not active, as indicated by the potentially unstable layer created by cloud-top radiative cooling, the entrained entities have time to circulate inside the cloud layer with continuous mixing with surrounding cloudy air that will lead to the broadening of droplet spectra.

These mechanisms should be represented in numerical models to accurately predict the evolution of marine boundary-layer cloud systems.

3. Project Outcomes and Publications

The DRI faculty and student participants of this project have prepared and published journal articles and presented conference papers resulting from the funded research. The PI served as a session chair at a conference related to this research. DRI has shared datasets resulting from this project with scientists at multiple institutions including NRL, University of Wyoming, UCLA and Oregon State University. Three graduate students have been partially supported by this project. The publications and presentations listed below have resulted in part or entirely from this project.

Adhikari, N.P., M.A. Wetzel, D.R. Koracin and S.K Chai, 2003: Analysis and prediction of microwave refractivity profiles in nocturnal marine cloud layers. Fifth Conference on Coastal Atmospheric Prediction and Processes. 8-12 August 2003, Seattle, WA, Amer. Meteor. Soc.

Chai, S.K., M.A. Wetzel, D. Koracin, D.-C. Kim and T. Sikora, 2004: Some observed characteristics of the marine boundary layer stratocumulus: Radiation and entrainment. Submitted to *J. Atmos. Sci.*

Chai, S.K., M.A. Wetzel and D. Koracin, 2003: Observed radiative cooling in nocturnal marine stratocumulus. Fifth Conference on Coastal Atmospheric Prediction and Processes. 8-12 August 2003, Seattle, WA, Amer. Meteor. Soc.

Gonzales, A., J.C. Perez, F. Herrera, R. Rosa, M.A. Wetzel, R.D. Borys and D.H. Lowenthal, 2001: Stratocumulus properties retrieval method from NOAA-AVHRR data based on the discretization of cloud parameters. *Intl. J. Rem. Sens.*, **23**, 627-645.

Haack, T., M. Wetzel and S.D. Burk, 2004: Marine Atmospheric Boundary Layer Clouds along the U.S. West coast from a mesoscale model reanalysis. To be submitted to *Monthly Weather Review.*

Koracin, D., J. Powers, M.A. Wetzel, S. Chai and N. Adhikari, 2003: Improving prediction of the marine coastal clouds using satellite and aircraft data. Fifth Conference on Coastal Atmospheric Prediction and Processes. 8-12 August 2003, Seattle, WA, Amer. Meteor. Soc.

Stevens, B., D.H. Lenschow, G. Vali, H. Gerber, A. Bandy, B. Blomquist, J.-L. Brenguier, C.S. Bretherton, F. Burnet, T. Campos, S. Chai, L. Faloona, D. Friensen, S. Haimov, K. Laursen, D.K. Lilly, S.M. Loehrer, S.P. Malinowski, B. Morely, M.D. Peners, D.C. Rogers, L. Russell, V. Savic-Jovcic, J.R. Snider, D. Straub, M.J. Szumoswki, H. Takagi, D.C. Thorton, M. Tshudi, C. Twohy, M. Wetzel, and M.C. Van Zanten, 2002: Dynamics and chemistry of marine stratocumulus -- DYCOMS-II. *Bull., Amer. Meteor. Soc.*, **84**, 579-593.

Twohy, C.H., M.D. Petters, J.R. Snider, B. Stevens, W. Tahnk, M. Wetzel, L. Russell, J.-L. Brenguier, 2005: Measurements of the indirect effect of aerosol particles on marine stratiform clouds: Microphysics. In press, *J. Geophys. Res.*

Vellore, R.K., D. Koracin, M. Wetzel and J.G. Powers, 2004: Verification study: Modeling the evolution and structure of nocturnal marine stratocumulus during DYCOMS-II. Accepted for presentation, Sixth Conf. on Coastal Atmospheric and Oceanic Prediction and Processes, Amer. Meteor., Soc.

Vellore, R.K., D.K. Koracin, M.A. Wetzel and J.G. Powers, 2004: Numerical modeling of cloudy boundary layer in the U.S. West Coast: The skill and improvement in the planetary boundary parameterizations. *In preparation.*

Vellore, R.K., D.K. Koracin, M.A. Wetzel, S.K. Chai and J.G. Powers, 2004: Improving mesoscale modeling of marine coastal clouds using satellite and aircraft data. *In preparation.*

Wetzel, M.A., G. Vali, W. Thompson, S.K. Chai, T. Haack, M. Szumowski and R.Kelly, 2001: Evaluation of COAMPS forecasts using satellite retrievals and aircraft measurements. *Weather and Forecasting*, **16**, 588-599.

4. Additional References

Bretherton, C.S. and co-authors, 1999: An intercomparison of radiatively driven entrainment and turbulence in a smoke cloud, as simulated by different numerical models. *Quart. J. Roy. Meteor. Soc.*, **125**, 391-423.

Deardorff, J.W., 1976: On the entrainment rate of a stratocumulus-topped mixed layer. *Quart. J. Roy. Meteor. Soc.*, **102**, 563-582.

Deardorff, J.W., 1980: Cloud-top entrainment instability. *J. Atmos. Sci.*, **37**, 131-147.

Haack, T. and S.D. Burk, 2001: Summertime marine refractivity conditions along coastal California. *J. Appl. Meteor.*, **40**, 673-687.

Lilly, D.K., 1968: Models of cloud-topped mixed layers under a strong inversion. *Quart. J. Roy. Meteor. Soc.*, **94**, 292-309.

Lock, A.P. and M.K. MacVean, 1999: The parameterization of entrainment driven by surface heating and cloud-top cooling. *Quart. J. Roy. Meteor. Soc.*, **125**, 271-299.

Randall, D.A., 1980: Conditional instability of the first kind upside-down. *J. Atmos. Sci.*, **37**, 125-130.

Rossow, W.B., and L.C. Garder, 1993: Validation of ISCCP cloud detections. *J. Climate,* **6**, 2370- 2393.

Rozendaal, M. A., C. B. Leovy, and S. A. Klein, 1995: An observational study of diurnal variations of marine stratiform cloud. *J. Climate*, **8**, 1795-1809.

Stevens, D.E., J.B., Bell, A. S. Almgren, V.E. Beckner, and C.A. Rendleman, 2000: Small-scale processes and entrainment in a stratocumulus marine boundary layer. *J. Atmos. Sci.*, **57**, 567-580.

Telford, J. W. and S. K. Chai, 1980: A new aspect of condensation theory. *Pure Appl. Geophys.*, **118**, 720-742.

Telford, J. W. and P. B. Wagner, 1981: Observations of condensation growth determined by entity type mixing. *Pure Appl. Geophys.*, **119**, 934-965.

Telford, J.W. and S.K. Chai, 1984: Inversions, and fog, stratus and cumulus formation in warm air over cooler water. *Bound.-Layer Meteor.*, **29**, 109-137.

Telford, J. W., T. S. Keck, and S. K. Chai, 1984: Entrainment at cloud tops and the droplet spectra. *J. Atmos. Sci.*, **41**, 3170-3179.

Telford, J. W. and S. K. Chai, 1993: Vertical mixing in clear air and clouds. *J. Appl. Meteor.*, **32**, 700-715.